In Situ Depositing Silver Nanoclusters on Silk Fibroin Fibers Supports by a Novel Biotemplate Redox Technique at Room Temperature

Qun Dong,† Huilan Su,* and Di Zhang‡

State Key Laboratory of Metal Matrix Composites, Shanghai Jiaotong University, Shanghai 200030, P. R. China

Received: May 28, 2005; In Final Form: July 28, 2005

Evolvement of bioinspired approaches for the construction of well-ordered nanostructures is a crucial intersection of branches of materials science and biotechnology. In this paper, floriated clusters of silver nanocrystallites, which consist of polycrystalline grains about 5 nm in diameter, have been successfully prepared on silk fibroin fibers (SFFs) through an in situ biotemplate redox approach at room temperature. The reductive amino acid tyrosine of SFFs mainly provided both reduction and location functions under alkaline conditions and could reduce Ag(I) ions to Ag(0). Finally, stable silver nanoclusters were generated on SFF substrates. The morphologies of silver nanoclusters were mostly attributed to the concentration of silver nitrate solution as well as special configurations and structures of silk fibroin macromolecules. A possible mechanism was explored intensively for tyrosine-residue-based silver nanocrystal formation.

Introduction

Where nature finishes producing its own species, man begins, using natural things, with the help of this nature, and creates an infinite number of species. These words epitomizing the artist−scientist Leonardo da Vinci fully embody the competence of human beings to utilize natural substances for synthesizing new materials. More and more researchers have turned to nature for inspiration, now that there exists an abundance of bioorganisms with organized fancy structures and supernatural virtues, which may gestate inorganic functional materials either intra- or extracellularly.[1,2] The secrets gleaned from nature have led to the development of biomimetic approaches for advanced nanomaterials with hierarchical structures. Some biological materials, for instance, oyster shells,[3] diatoms,[4] sea urchin spines,[5] cuttlefish bone,[6] nacre,[7] egg shell membrane,[8] DNA chains,[9] viruses,[10] and peptide nanotubes,[11] were utilized to prepare organic−inorganic composites or inorganic hierarchical materials. Thereinto, more attention has been focused upon building noble metal nanostructures due to their unusual optical properties as well as their novel chemical and catalytic properties, combining characteristic hierarchical structures.[12−14]

Actually, the utilization of biological organisms has emerged as a novel method for the synthesis of noble metal nanoparticles. In a break from tradition, it has hitherto relied more on the use of prokaryotes such as bacteria, viruses, and so on, as well as proteins, recurring to the intracellular synthesis of silver nanoparticles. Ahmad and co-workers have shown that eukaryotic organisms such as fungi could be extremely good candidates for the synthesis of Ag nanoparticles.[15,16] The biosynthesis of silver nanoparticles has also been achieved using peptides with the ability to bind silver ions and particles.[17] Moreover, it has been published that some living plants, such as Alfalfa sprouts[18] and Geranium leaf,[19] had the capability to take up silver ions from solid media and produce silver nanoparticles resulting in the possibility of an environmentally friendly method of recovering precious metals from mining wastes and a new alternative for the production of nanoparticles. All the processes could be easily controlled under mild and ecofriendly conditions. Here, silver nanoparticles are chosen as the candidate linked to the biotemplate, with a view that silver particles with nanoscale building blocks have received a great deal of attention recently, owing to their promising applications in modern science and technology,[20−23] for example, electron microscopy (contrast agents),[24] analysis (chemical and biological sensors),[25] electronics (single-electron transistors, electrical connects),[26] materials (dyes, conductive coatings),[27] and even catalysis.[28] Whereas silver nanoparticles usually exist as colloids in the liquid system, which restricts the applications in some domains, for example, as the solid catalyst as the catalysis relies on the sizes and morpologies of both silver particles and solid supports, as well as their reciprocities. It is extremely difficult to find an appropriate solid support on which Ag(I) ions can be reduced to Ag(0) at ambient temperature.[29] However, it may be achieved by selecting the proper biological template as the substrate, on which silver nanoparticles can be deoxidized and grown in situ. A convenient biomaterial silk extracted from the silkworm *Bombyx mori* cocoons, what with redox-active silk fibroin fibers (SFFs) containing manifold amino acids and chemical residues, among which the tyrosine residue (Tyr) component has strong electron donating complex properties, should been given priority for the preparation of noble metal nanomaterials through biotemplate techniques under mild conditions. It was demonstrated that silk fibers could induce apatite deposition on the surfaces of proteins.[30] Kong and co-workers utilized silk fibers after degumming sericin as the organic template to regulate the mineralization of calcium phosphate.[31] Elicited for the bioinspiration, we did not redissolve the silk into silk fibroin (SF) proteins, which was different from the research on the reduction of Au with dissolved SF proteins,[32] but we directly utilized SFF as the reductive template to synthesize silver nanostructures. In the present work, silver/silk composites with the degummed

* To whom correspondence should be addressed. Tel.: +86-21-62932122. Fax: +86-21-62822012. E-mail: hlsu@sjtu.edu.cn.
† E-mail: dongqun@sjtu.edu.cn.
‡ E-mail: zhangdi@sjtu.edu.cn.

10.1021/jp052826z CCC: $30.25 © 2005 American Chemical Society
Published on Web 08/25/2005

SFFs from silkworms have been successfully prepared through a biotemplate redox-active technique, in which Tyr residues on SFFs provide both reduction and location functions, and silver nanocrystallites present special cluster microstructures owing to the unique array of SFFs. It is more convenient to prepare silver nanoclusters on the reductive biotemplate SFF supports under ambient conditions. This method and the relevant ideas offer a path to fabricate advanced functional materials with novel topologies.

Experimental Section

Cocoons of *B. mori* silkworm were kindly supplied by Shanghai Natural Wild-Insect Kingdom Co., Ltd. Analytic grade reagents Na_2CO_3, NaOH, and $AgNO_3$ were purchased from Shanghai Chemical Company. Redox-active SFF was obtained by removing the sericin, the gummy binding protein coating the silk fibroin filaments, from original silks with the degumming process involving boiling the cocoons in 0.05 M Na_2CO_3 solution. The degummed SFF contains negligible residual silk wax and sericin.[33] It was dried in a vacuum overnight at 80 °C and stored in the dark under vacuum at room temperature in order to avoid degradation. In a typical experiment, silver nitrate solution with volumes 20, 5, 1, and 0.2 mL of 0.01 M were injected into conical flasks and diluted to 100 mL, respectively. A certain amount of SFF ca. 8.5 mg was immersed into the solutions in the dark. The bio-reduction of silver ions on SFF substrates was monitored by periodic sampling of aliquots (2 mL) of the aqueous component and measuring the UV−vis spectrum of the solution.

UV−vis spectra of these aliquots were monitored on a Perkin-Elmer Lambda 20 spectrophotometer operating at a resolution of 0.3 nm. X-ray diffraction (XRD) measurements of SFF and Ag/SFF were carried out on a Bruker-AXS D8 Advance instrument operating at a voltage of 40 kV and a current of 40 mA with Cu Kα radiation ($\lambda = 1.5406$ Å). For Fourier-transform infrared (FTIR) spectroscopy measurements, spectra of original specimen SFF and Ag/SFF composites after 4 h reaction were recorded on a Nicolet NEXUS-670 instrument with an attenuated total reflectance Fourier transform (ATR-FTIR) by accumulation of 32 scans at a resolution of 4 cm^{-1} and a spectral range 7400−350 cm^{-1}. For further investigation of the synthesis process, magic-angle spinning (MAS) solid-state nuclear magnetic resonance (NMR) spectroscopy measurements were performed on a Varian MERCURY plus 400 MHz instrument and scanned in the range 0−200 ppm with ^{13}C cross-polarization (CP) MAS spectra (100.6 MHz, 2.5 ms CP time, 2100 scans). Images of Ag/SFF composites were obtained with a FEI Sirion 200 field emission gun scanning electron microscope (FESEM). Transmission electron microscopy (TEM) measurements were performed on a JEOL-100CX transmission electron microscope operated at an accelerating voltage of 100 kV.

Results and Discussion

In situ reduction of the aqueous Ag(I) ions on degummed SFF supports can track UV−vis spectroscopy. Figure 1 shows the UV−vis spectra recording SFF and Ag/SFF solutions with different concentrations of Ag(I) ions. Figure 1A clearly shows that pure SFF does not absorb in the visible region. It is observed from Figure 1B that the surface plasmon resonance band occurs at ca. 410 nm with addition of 20 mL of $AgNO_3$ solution kept for 4 h in the dark. Since silver nanoparticles are known to exhibit a size-dependent characteristic surface plasmon resonance band that can be measured, the characteristic absorption might be due to the redox of the Tyr component in SFF in the case of the $AgNO_3$ solution and the formation of silver nanoparticles, which is further proved by XRD results, and this absorption arises due to excitation of surface plasmons in the nanoparticles.[34] Actually, it has been reported that the amino acid Tyr is an excellent reducing agent only under alkaline conditions.[35] However, it is not inconsistent with the current result owing to the pretreatment of SFF in Na_2CO_3 solution (a base medium) making for the ionization of the phenolic group of Tyr. Pretreated SFF thus had reduction activation and could nucleate silver nanocrystallites in situ on SFF supports, regardless of rigorous pH value. Although the total content of Tyr only comes up to 5.17 mol % of silk fibroin, the Tyr is mainly located around SFF for its complex aromaticity, which might reduce silver ions around the membrane as the role of biotemplate. If the addition of $AgNO_3$ solution is increased above 20 mL, Figure 1C shows that the intensity of this plasmon peak changes very little with a blue shift, and a new peak appears at 570 nm. The two peaks, respectively, could be attributed to the transverse and longitudinal plasmon resonance of rod-shaped silver nanostructures.[36] However, no evident peaks could be tracked with the addition of $AgNO_3$ solution less than 1 mL due to the formation of few silver nanoparticles. It is considered that 4 h was enough, and the volume of 0.01 M $AgNO_3$ solution should range from 1 to 20 mL for the synthesis of silver nanocrystallites on SFF supports.

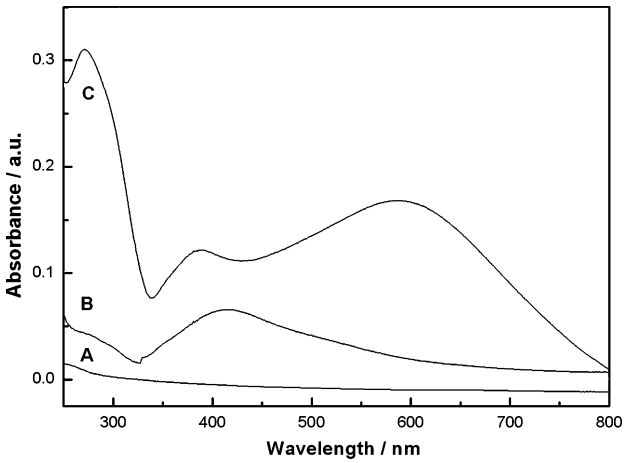

Figure 1. UV−vis absorption spectra of the aqueous solutions of (A) SFF and (B, C) Ag/SFF with the additions of 20 mL and above 20 mL of 0.01 M $AgNO_3$ kept in the dark for 4 h at room temperature.

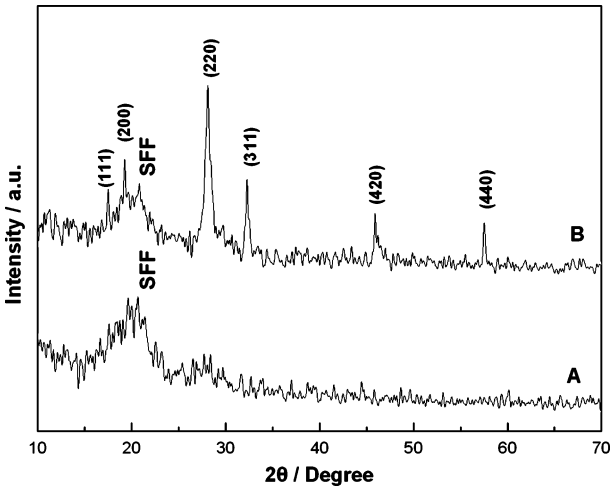

Figure 2. XRD patterns of (A) the original degummed silk and (B) silver nanoparticles on SFF supports. The Bragg reflections are indexed on the basis of the fcc Ag structure.

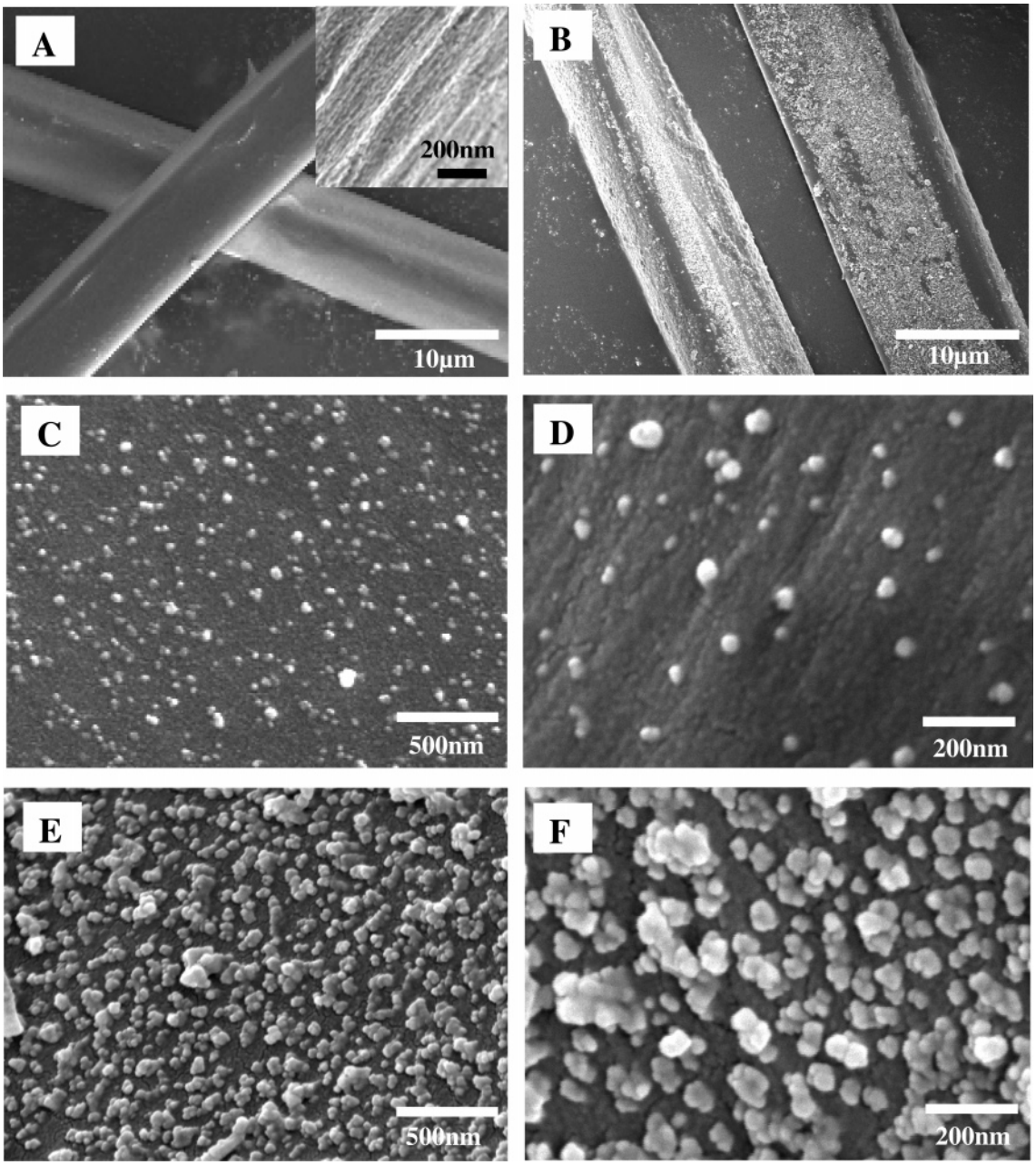

Figure 3. FESEM images of (A) the original SFF template, with the inset showing high magnification of the surface skin coat of aligned protein compared with the panorama of Ag/SFF composites, silver nanoparticles on SFF supports with different dosages of 0.01 M $AgNO_3$ as the reagents, (C) and (D) 1 mL, (B), (E), and (F) 20 mL. Images in parts D and F show high magnifications of parts C and Figure E, respectively.

Figure 2A,B shows the XRD patterns of SFF substrates and Ag/SFF composites, respectively. It can be seen that pure SFFs containing plenty of amines, amides, and carboxylic surface functional groups were nearly amorphous whereas glycine-X repeats covering 94% of the silk sequence (X is alanine in 65%, serine in 23%, and tyrosine in 9% of the repeats),[37] mainly forming crystalline domains in silk fibers resulting in the peak around 20.64°.[38] A number of prominent Bragg reflections can be seen in Figure 2B that could be indexed as the face-centered cubic (fcc) structure of silver with the corresponding diffraction peaks of (111), (200), (220), (311), (420), and (440) planes. The reflection peaks appear broader indicating as-prepared silver nanoparticles with small dimensions, which is in agreement with UV−vis spectra results.

Figure 3A shows the characteristic FESEM images of original SFF supports, which seem as clean as a whistle under low magnification (see Supporting Information, Figure 1S), as the surface skin coat of aligned protein obviously appears in the magnified images in the inset of Figure 3A. It reveals that the surface has a regular rugged framework containing proteins chains with certain chemical residues. Figure 3B shows the typical images of silver nanoparticles depositing on SFF supports for 4 h, contrasting against the original SFF supports shown in Figure 3A observed from the panorama. One can see that silver nanoparticles distribute uniformly on SFF substrates. As a general rule, it is necessary to precisely control the reaction conditions, for example, the concentration of the silver ions, besides the base system during degumming process using Na_2CO_3 solution. Figure 3C,D and Figure 3E,F show the images of Ag/SFF with 1 mL and 20 mL 0.01 M $AgNO_3$ solution as the reactants, respectively. Under low concentration (with 1 mL of $AgNO_3$ added), as-prepared silver nanoparticles distribute uniformly and present a spherical shape with a mean size of ca. 21 nm shown in Figure 3C; few grow up exceptionally as

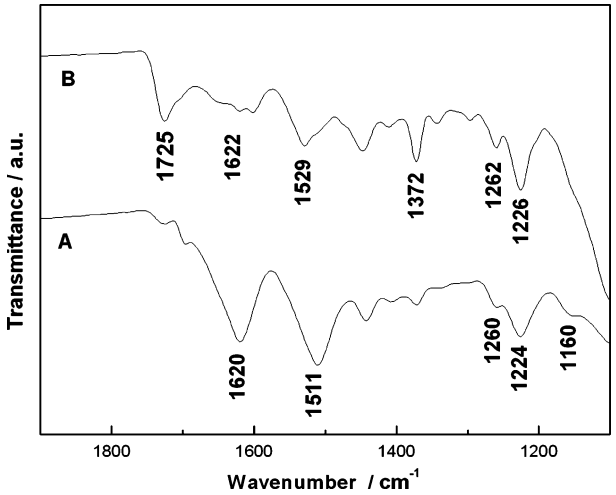

Figure 4. ATR-FTIR spectra of (A) original degummed silk and (B) silver nanoparticles on SFF supports.

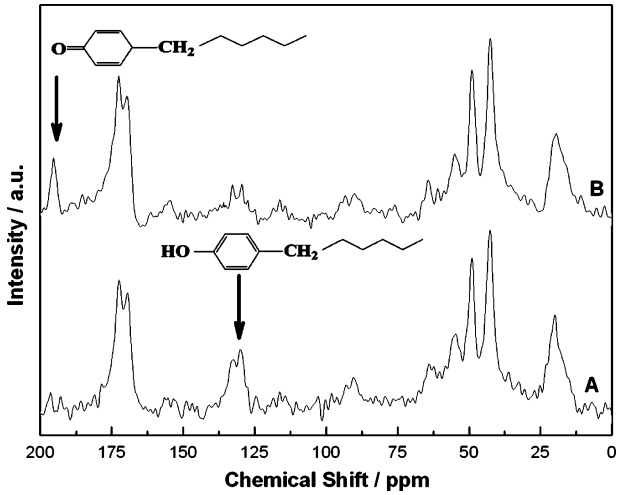

Figure 5. MAS solid-state NMR spectra of (A) original degummed silk and (B) silver nanoparticles on SFF supports. The inset shows a transformation of the functional structure of Tyr component, which is a consequence of the reduction of silver ions and formation of silver nanoparticles.

shown in Figure 3D. Figure 3E,F shows that silver nanocrystallites come into being ca. 30−50 nm clusters with the floriated figuration conjoined by about 5 nm small grains, as the silver ion concentration is elevated (with 20 mL of $AgNO_3$ added). It indicates that an increase in silver ion concentration leads to an obvious morphologic evolution of silver nanostructures from dispersed grains to nanoclusters, which would be likely caused by the interactions of dissociative silver ions and the chemical residues of SFF supports.

To further explore the in situ deposition process, ATR-FTIR measurements were carried out to identify possible biochemical radicals among biomolecules, which could be responsible for the reduction of Ag ions and capping silver nanoparticles. The degummed SFF supports were extracted from the solution and subsequently rinsed with distilled water and absolute alcohol, respectively. Finally, the fibers were collected for FTIR analysis. Figure 4A represents the FTIR spectrum of degummed silks and shows the diagnostic peaks at 1620, 1511, and 1224 (connected 1260) cm^{-1}. These peaks are assigned to the amide I, amide II, and amide III (crystal region, 1224 cm^{-1}; amorphous zone, 1260 cm^{-1}) bands of proteins released by SFF, respectively, which predominantly indicate β-sheet structure. The peaks at 1443 and 1372 cm^{-1} may be assigned to symmetric stretching vibrations of carboxylate groups of amino acid residues with free carboxylate groups and methylic groups of alanine in the proteins. The peaks at 1620 and 1160 cm^{-1} arise from a carbonyl stretching vibration and phenolic groups of Tyr, respectively, which shows the carbonyl stretching vibration from the carboxylate ions and the hydroxyl stretching vibration from the phenolic ions in Tyr of the pure SFF. As for Figure 4B, the peak of SFF at 1160 cm^{-1} disappears which indicates the phenolic residue exhausted, simultaneity showing the carbonyl stretching vibration peak at 1725 cm^{-1}, which may be attributed to the formation of a quinone structure due to oxidation of the phenolic group in Tyr. It has been reported that proteins can bind to metal nanoparticles through either free amine groups or cysteine residues in the proteins.[39] In these circumstances, oxidized tyrosine molecules bounded Ag crystallites through amine groups so that Ag nanoparticles could stabilize, and this is also supported by the shift of the characteristic peaks. The amide I band at 1620 cm^{-1} has broadened, which also indicates the capping manner of silver nanoparticles by SFF macromolecules.

It has been further confirmed by MAS solid-state NMR analysis of pure SFF (Figure 5A) compared with Ag/SFF (Figure 5B). The resonances of the phenyl group of Tyr is usually measured to be at 130−150 ppm (shown by an arrow in Figure 5A), assigned to sp^2-hybridized carbons of a phenyl group replaced by a hydroxy group. Due to the oxidation of Tyr components, the phenyl group is converted into a semiquinone; the chemical shift of quinone ^{13}C is measured to be in the region of 180−190 ppm (Figure 5B) while the resonances at 160−170 ppm just arose by the C of carbonyl in the carboxyl residues of SFF. In the case of Ag/SFF, a peak at 189 ppm (shown by a arrow in Figure 5B) should be corresponding to semiquinone hailing from the phenyl group during the reduction of Ag(I) to Ag(0). This peak is clearly missing in the NMR spectrum of pure SFF (Figure 5A). On the basis of these observations, the corresponding chemical structure transformation of Tyr components of SFF can be described in the inset of Figure 5.

As proven in the preceding text, it is ensured that the redox-active Tyr residues, mainly located around the surface of SFF, would farthest reduce silver ions on account of the ionization of SFF during the pretreatment under alkaline conditions. A tentative degummed process substituting distilled water for 0.05 M Na_2CO_3 solution could not bring off ionization, and there presented no evident silver grains, which indirectly proved that the reducing ability of Tyr was achieved predominantly in an alkaline system. Thus, the reducing capability of Tyr was enhanced for the phenolic group of Tyr at high pH. Consequently, the silver ions could be reduced by amines and amides and interacted with carboxylic surface functional groups contained in those protein chains around SFF substrates. The redox process would occur in the present case between phenolic groups of Tyr exposed from SFF and captured Ag(I) ions; ultimately, Ag nanoclusters could stabilize on SFF.

We proposed the model presented in Scheme 1 for Tyr-residue-based silver nanocrystal formation; however, the morphologies of silver nanoclusters rely on special macromolecule structures of the biotemplate SFF as well as on silver ion concentration. The fibroin is an insoluble protein containing up to 90% of the amino acids glycine, alanine, serine, and tyrosine, leading to a significant amount of antiparallel β-pleated sheet formation in the fibers.[38] On examination of the primary sequence for the fibroin heavy chain, a pattern of hydrophobic and hydrophilic blocks has been identified that includes larger hydrophilic blocks at the chain ends, and smaller hydrophilic

SCHEME 1: Illustration of In Situ Deposition of Ag Nanoparticles on SFF Biotemplate for Different Morphologies and Arrangements Relying on the Concentration of Silver Ions and Macromolecule Structures of SFF[a]

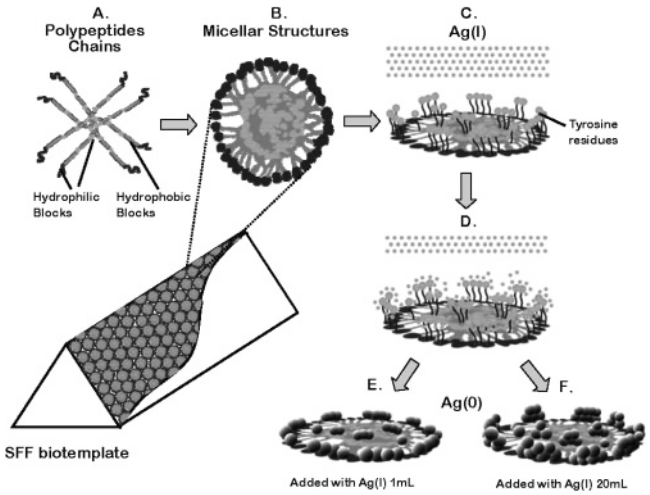

[a] Models of (A) chain folding, (B) micelle formation, and (C, D) the reaction of silver ions with chemical residues bringing out two morphologies formed under different dosages of 0.01 M $AgNO_3$ as the reagents, (E) 1 mL and (F) 20 mL, respectively.

blocks and hydrophobic blocks jointed at intervals as described in Scheme 1A. This pattern suggests the possibility of forming micellar structures in liquid systems (Scheme 1B).[40] Fibroin molecules acted as the hydrophilic−hydrophobic−hydrophilic polymers, during the formation of irregular sized micelles depending on chain folding and hydrophobic interactions. The smaller hydrophilic blocks would remain hydrated, and the larger terminal hydrophilic blocks at both the amino and carboxy termini defined the outer edges of the micelles. Tyrosine residues are distributed according to the silk sequence of the amino acids and are present all the way through the molecule, both in the hydrophilic and hydrophobic regions. Here, the organization does not give significant spatial ordering of the tyrosine. Distributed locations of Tyr residues were calculated according as the GX repeats forming the bulk of the polypeptide chain (see Supporting Information, Figure 2S). Clearly, Tyr residues do not distribute in a well-proportioned way but behave as separated tufts at ca. 20−50 nm level shown in Scheme 1C. Through coulombic interactions, the Ag(I) ions could be captured by phenolic groups of chemical residues. With this premise, the concentration of silver ions would affect the morphologies of as-prepared silver nanoparticles as shown in Scheme 1E,F. Under higher concentrations, as-formed silver crystallites present shapely spheres with ca. 5 nm size, due to homogeneous nucleation of ample silver ions. It is worth noting that silver nanoparticles grow into nanoclusters as shown in Figure 3E,F. Tyrosine residues on SFF could contribute to the formation of silver nanoparticles in both reduction and location. Hence, peculiar structures of Tyr residues and SFF would be responsible for directing some morphological controls over the placement of silver nanocrystals. The interaction of Tyr residues with silver nuclei provides a chemically reducing environment, thereby allowing further accelerated reduction of silver ions with sufficient metal ions at the interface between Tyr residues and silver nanoparticles. It exists as continuous growth by the diffusion of species from the solution with a great deal of silver ions toward the surfaces of primeval nuclei which are built up into combined series leading to floriated cluster morphology. There are intervals between every two Tyr residues, aggregations as shown in Figure 3 F, which are consistent with the distributing locations of Tyr residues. Although the reductive reaction is the same as the former, a lower concentration of silver ions generates a single, long burst of nuclei; these nuclei could be bound by Tyr and slowly grow up, as shown in Figure 3C,D. In some areas, a broad range of size distribution indicates the occurrence of multiple nucleation events.[41] Some silver nanoparticles with the size of ca. 45 nm are formed anisomerously due to the transitory undulation of silver ion concentration. Other results, e.g., some FESEM images (see Supporting Information, Figure 3S and Figure 4S), also convincingly support the model. Silver nanoparticles would present in interrupted arrays, in the respect that amino acid residues such as arginine, cysteine, lysine, and methionine are known to interact with silver ions,[17] which leads to the faulty arrangement differing from the ideal state. In any case, the interactions among protein blocks, as well as distributing and spacing of these residues, play a critical and complicated role in the nucleation and growth of silver nanocrystallites. Thus, silver nanoparticles present in arrays unconspicuously or in an out-of-order array.

Representative TEM images of as-prepared silver nanoparticles separated from SFF and ones sticking on SFF proteins are shown in Figure 6A,B (with 20 mL of silver nitrate solution added), respectively. These reveal that silver crystallites show themselves as nanoclusters. The SAED pattern shown in the inset of Figure 6A reveals that the particles are polycrystalline in nature and the rings could be indexed as the fcc structure of

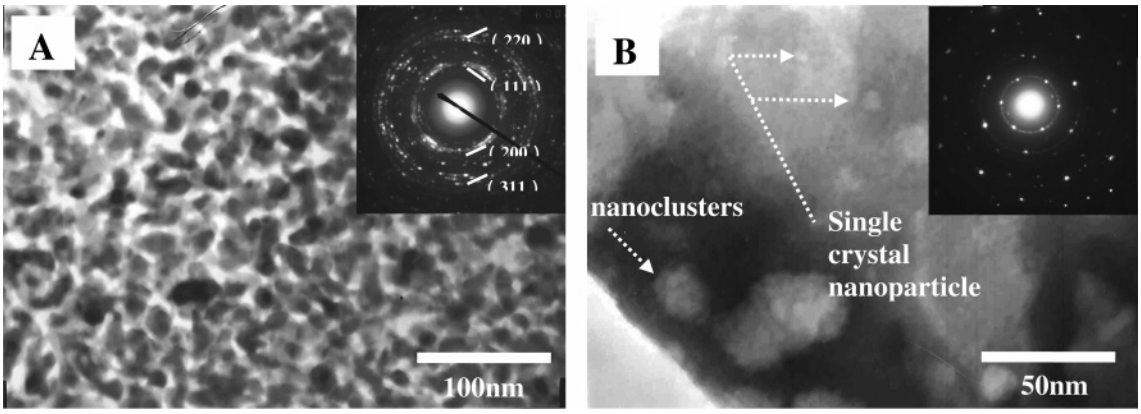

Figure 6. Representative TEM images of as-prepared Ag nanoclusters (added with 20 mL of 0.01 M $AgNO_3$). Part A shows Ag nanoclusters separated from SFF substrates. The inset in part A shows the selected area electron diffraction (SAED) pattern of the nanoclusters. Part B shows Ag particles sticking on SFF proteins. The inset in part B shows the convergent beam electron diffraction patterns recorded by directing the electron beam perpendicular to the (111) facet.

crystalline silver, which is consistent with the XRD results of Figure 2. As shown in Figure 6B, there are few spherical nanoparticles with a size of 10 nm on SFF proteins, and these special particles are indexed to single-crystalline silver as shown in the inset of Figure 6B. The uniformity in size for as-formed nanocrystallites could have been achieved through a self-sharpening growth process during which small particles grow more rapidly than larger ones. In addition, it is found that silver nanoparticles combined into larger swarms with ultraviolet radiation. A number of recent studies suggested that it should rather be the conglomeration of some smaller subunits (or primary crystallites) than continuous growth by the diffusion of species from the solution toward the surfaces of nuclei.[41] The as-prepared silver nanoclusters are rather stable on SFF supports over a period of several months, even under knocking on SFF substrates.

Conclusions

An efficient and convenient biochemical pathway has been successfully developed for the synthesis of silver nanoparticles/SFF composites, with silk fibroin fibers as the biotemplate, support, and reducer. The loading of silver nanoparticles is as high as 60% of the whole surface area, and it is clear that the "biomaterial frameworks" provided highly effective sites for deoxidization and loading of noble metal nanoparticles, composing structures of macroscopic to nanoscopic dimensions. We could ensure large surface areas, highly uniform metal loading, and enhanced particle stability in such hierarchical morphology. The biosynthesis of such complex loading is rendered predominantly by using appropriate hierarchical and chemical templates, and should be extremely beneficial from practical standpoints. The present approach can produce versatile nanostructured systems with unique physical and chemical functions; foremost, it is felicitous to find an appropriate solid support that can reduce silver ions to silver particles at ambient temperature. Our discovery that Tyr of SFF provides a redox-active framework to construct nanostructured silver crystallites is an important advance in combining biotemplate and chemical synthesis in the direction of organic−inorganic advanced materials synthesis.

Acknowledgment. This work was supported by the financial support of the Major Fundamental Research Project, Shanghai Science and Technology Committee under Grant 04DZ14002, and Shanghai Nanotechnology Center under Grant 0352NM051.

Supporting Information Available: FESEM images showing prism figure of original SFF substrates; distributing locations of Tyr residues according to the GX repeats of the amino acid sequence of the silk fibroin heavy chain; and FESEM images of silver nanoparticles on SFF substrates with 1 mL and 20 mL of 0.01 M $AgNO_3$ as the reagents. This material is available free of charge via the Internet at http://pubs.acs.org.

References and Notes

(1) Simkiss, K.; Wilbur, K. M. *Biomineralization*; Academic Press: New York, 1989.
(2) Mann, S. E. *Biomimetic Materials Chemistry*; VCH Publishers: New York, 1996.
(3) Li, X. D.; Chang, W. C.; Chao, Y. J.; Wang, R.; Chang, M. *Nano Lett.* **2004**, *4*, 613.
(4) Weatherspoon, M. R.; Allan, S. M.; Hunt, E.; Cai, Y.; Sandhage, K. H. *Chem. Commun.* **2005**, 651.
(5) Seshadri, R.; Meldrum, F. C. *Adv. Mater.* **2000**, *12*, 1149.
(6) Ogasawara, W.; Shenton, W.; Davis, S. A.; Mann, S. *Chem. Mater.* **2000**, *12*, 2835.
(7) Sellinger, A.; Pilar, Weiss, P. M.; Nguyen, A.; Lu, Y. F.; Assink, R. A.; Gong, W. L.; Brinker, C. J. *Nature* **1998**, *394*, 256.
(8) Yang, D.; Qi, L. M.; Ma, J. M. *Adv. Mater.* **2002**, *14*, 1543.
(9) Le, J. D.; Pinto, Y.; Seeman, N. C.; Karin, M. F.; Taton, T. A.; Kiehl, R. A. *Nano Lett.* **2004**, *4*, 2343.
(10) Lee, S. W.; Mao, C. B.; Flynn, C. E.; Belcher, A. M. *Science* **2002**, *296*, 892.
(11) Reches, M.; Gazit, E. *Science* **2003**, *300*, 625.
(12) Lutich, A. A.; Gaponenko, S. V.; Gaponenko, N. V.; Molchan, I. S.; Sokol, V. A.; Parkhutik, V. *Nano Lett.* **2004**, *4*, 1755.
(13) Berry, V.; Rangaswamy, S.; Saraf, R. F. *Nano Lett.* **2004**, *4*, 939.
(14) Sheeney-Haj-Ichia, L.; Pogorelova, S.; Gofer, Y.; Willner, I. *Adv. Funct. Mater.* **2004**, *14*, 416.
(15) Mukherjee, P.; Ahmad, A.; Mandal, D.; Senapati, S.; Sainkar, S. R.; Khan, M. I.; Parischa, R.; Ajayakumar, P. V.; Alam, M.; Kumar, R.; Sastry, M. *Nano Lett.* **2001**, *1*, 515.
(16) Shankar, S. S.; Ahmad, A.; Pasricha, R.; Sastry, M. *J. Mater. Chem.* **2003**, *13*, 1822.
(17) Naik, R. R.; Stringer, S. J.; Agarwal, G.; Jones, S. E.; Stone, M. O. *Nat. Mater.* **2002**, *1*, 169.
(18) Gardea-Torresdey, J. L.; Gomez, E.; Peralta-Videa, J. R.; Parsons, J. G.; Troiani, H.; Jose-Yacaman M. *Langmuir* **2003**, *19*, 1357.
(19) Shankar, S. S.; Ahmad, A.; Sastry, M. *Biotechnol. Prog.* **2003**, *19*, 1627.
(20) Jin, R. C.; Cao, Y. W.; Mirkin, C. A.; Kelly, K. L.; Schatz, G. C.; Zheng, J. G. *Science* **2001**, *294*, 1901.
(21) Kim, S. W.; Kim, M.; Lee, W. Y.; Hyeon, T. *J. Am. Chem. Soc.* **2002**, *124*, 7642.
(22) Liang, H. P.; Zhang, H. M.; Hu, J. S.; Guo, Y. G.; Wan, L. J.; Bai, C. L. *Angew. Chem., Int. Ed.* **2004**, *43*, 1540.
(23) Zhang, D. B.; Qi, L. M.; Ma, J. M.; Cheng, H. M. *Adv. Mater.* **2002**, *14*, 1499.
(24) Hayat, M. A. *Colloidal gold: principles, methods, and applications*; Academic Press: San Diego, 1989.
(25) Krasteva, N.; Besnard, I.; Guse, B.; Bauer, R. E.; Mullen, K.; Yasuda, A.; Vossmeyer, T. *Nano Lett.* **2002**, *2*, 551.
(26) Klein, D. L.; McEuen, P. L.; Bowen-Katari, J. E.; Roth, R.; Alivisatos, A. P. *Appl. Phys. Lett.* **1996**, *68*, 2574.
(27) Musick, M. D.; Keating, C. D.; Lyon, L. A.; Botsko, S. L.; Pena, D. J.; Holliway, W. D.; McEvoy, T. M.; Richardson, J. N.; Natan, M. J. *Chem. Mater.* **2000**, *12*, 2869.
(28) Pietron, J. J.; Stroud, R. M.; Rolison, D. R. *Nano Lett.* **2002**, *2*, 545.
(29) Hong, B. H.; Bae, S. C.; Lee, C. W.; Jeong, S.; Kim, K. S. *Science* **2001**, *294*, 348.
(30) Takeuchi, A.; Ohtsuki, C.; Miyazaki, T.; Ogata, S.; Tanihara, M.; Tanaka, H.; Furutani, Y.; Kinoshita, H. *Key Eng. Mater.* **2003**, *240*−*2*, 31.
(31) Kong, X. D.; Cui, F. Z.; Wang, X. M.; Zhang, M.; Zhang, W. *J. Cryst. Growth* **2004**, *270*, 197.
(32) Zhou, Y.; Chen, W. X.; Itoh, H.; Naka, K.; Ni, Q. Q.; Yamane, H.; Chujo, Y. *Chem. Commun.* **2001**, 2518.
(33) Putthanarat, S.; Stribeck, N.; Fossey, S. A.; Eby, R. K.; Adams, W. W. *Polymer* **2000**, *41*, 7735.
(34) Kerker, M. *J. Colloid Interface Sci.* **1985**, *105*, 297.
(35) Selvakannan, P. R.; Swami, A.; Srisathiyanarayanan, D.; Shirude, P. S.; Pasricha, R.; Mandale, A. B.; Sastry, M. *Langmuir* **2004**, *20*, 7825.
(36) Sun, Y. G.; Gates, B.; Mayers, B.; Xia, Y. N. *Nano Lett.* **2002**, *2*, 165.
(37) Zhou, C. Z.; Confalonieri, F.; Jacquet, M.; Perasso, R.; Li, Z. G.; Janin, J. *Proteins* **2001**, *44*, 119.
(38) Rathore, O.; Sogah, D. Y. *Macromolecules* **2001**, *34*, 1477.
(39) Gole, A.; Dash, C.; Ramakrishnan, V.; Sainkar, S. R.; Mandale, A. B.; Rao, M.; Sastry, M. *Langmuir* **2001**, *17*, 1674.
(40) Jin, H. J.; Kaplan, D. L. *Nature* **2003**, *424*, 1057.
(41) Xia, Y. N.; Gates, B.; Yin, Y. D.; Lu, Y. *Adv. Mater.* **2000**, *12*, 693.